Sustainable Energy, Grids and Networks 43 (2025) 101861

Contents lists available at ScienceDirect

Sustainable Energy, Grids and Networks

journal homepage: www.elsevier.com/locate/segan

Optimal reconfiguration of radial distribution networks with renewable energy resources by considering configuration shift steps

Riccardo Nebuloni [a,*], Valentin Ilea [a], Cristian Bovo [b], Alberto Berizzi [a], Carlo Arrigoni [c], Filippo Re [c], Roberto Bonera [d]

[a] Department of Energy, Politecnico di Milano, Milano, Italy
[b] Department of Electrical, Computer, and Biomedical Engineering, Università degli Studi di Pavia, Pavia, Italy
[c] Grid Software Business Unit, Siemens SpA, Milano, Italy
[d] Freelancer, Milano, Italy

ARTICLE INFO

Keywords:
Distribution networks
Optimal network reconfiguration
Graph theory
Distributed energy resources
Zero-impedance branches

ABSTRACT

The optimal reconfiguration of distribution networks (DNs) is a critical strategy to improve the operational efficiency of modern power systems considering the increasing integration of renewable energy resources. Existing approaches, including heuristic algorithms and Mixed-Integer Linear Programming (MILP) techniques have demonstrated their relevance in addressing important objectives for DNs, such as loss minimization, feeder load balancing, and reliability maximization. However, these methods have some limitations, including single-time formulation, absence of explicit modeling of the transition steps during the shift period from the initial configuration to the optimal one, and the approximated representation of zero-impedance branches, which are necessary for accurate system modeling. This study introduces a novel MILP-based formulation for the multi-period optimal reconfiguration of DNs based on the knowledge of multi-temporal generation and load profiles. The model also considers practical operational constraints, including Rapid Voltage Change (RVC) limits and realistic switching sequences. In particular, the maneuvering process is explicitly modeled, enabling the identification of feasible transition paths while avoiding intermediate configurations that would violate network constraints. Moreover, an efficient formulation to include breakers and bus-ties as zero-impedance branches is developed, which improves the accuracy of the electrical model and ensures a more realistic representation of the DN topology. Simulation results on the IEEE 12-bus and IEEE 69-bus systems confirm the effectiveness of the approach: objective functions are close to ideal values even with a limited number of switching actions, while computation times remain below practical operational limits for the 69-bus test case, demonstrating the method's scalability and suitability for real-time operation.

1. Introduction

1.1. State of art and goals

In recent years, due to the pressing need for decarbonization, the European Union (EU) is pursuing strategies aimed at reducing greenhouse gas emissions [1]. Key initiatives include the implementation of the Renewable Energy Directive 2018/2001/EU [2], which sets a target for Renewable Energy Sources (RES) to cover 32 % of the energy mix by 2030 and the EU Directive 2019/1161 [3], which mandates that by 2025, 35 % of light-duty vehicles and 45 % of heavy-duty vehicles must be clean. Hence, the future of electric energy generation will be dominated by non-programmable RES, such as solar and wind power. As these sources become more relevant, they introduce new challenges in terms of grid stability and energy balancing, given their intermittent and unpredictable nature [4]. Studies have shown that this variability requires more flexible grid operations [5] and new market strategies [6]; in parallel, technological improvements are enabling more effective integration of RES, reinforcing their role as a primary component of future regulating frameworks [7]. Moreover, the transportation electrification, driven by the adoption of Electric Vehicles

* Corresponding author.
Email addresses: riccardo.nebuloni@polimi.it (R. Nebuloni), valentin.ilea@polimi.it (V. Ilea), cristian.bovo@unipv.it (C. Bovo), alberto.berizzi@polimi.it (A. Berizzi), carlo.arrigoni@siemens.com (C. Arrigoni), filippo.re@siemens.com (F. Re), roberto.bonera@gmail.com (R. Bonera).

https://doi.org/10.1016/j.segan.2025.101861
Received 15 December 2024; Received in revised form 28 March 2025; Accepted 23 July 2025
Available online 25 July 2025

Nomenclature

Sets

$t \in \mathbb{T}$ All considered time intervals
$\mathbb{T}^{op} \subset \mathbb{T}$ Time intervals of planned operation period
$\mathbb{T}^{c} \subset \mathbb{T}$ Time intervals of closing maneuvers
$\mathbb{T}^{o} \subset \mathbb{T}$ Time intervals of opening maneuvers
$\mathbb{T}^{s} \subset \mathbb{T}$ Time intervals of planned shift period $\mathbb{T}^{s} = \mathbb{T}^{c} \cup \mathbb{T}^{o}$
$k \in \mathbb{N}$ All nodes of the grid
$\mathbb{N}^{\nabla} \subset \mathbb{N}$ Nodes that are not the primary substations' HV nodes (slack)
$g \in \mathbb{G}$ All generators in the grid
$\eta^{\mathbb{G}}$ Node-generator connectivity map
$j \in \mathbb{B}$ All branches in the grid
$\mathbb{B}_k^{+} \subset \mathbb{B}$ Branches which, by current flow convention, are exiting from node k
$\mathbb{B}_k^{-} \subset \mathbb{B}$ Branches which, by current flow convention, are entering to node k
$\mathbb{B}^{Z_0} \subset \mathbb{B}$ Zero-impedance branches
$\mathbb{B}^{0} \subset \mathbb{B}$ First branches of the feeders, i.e. the ones connected to the primary substation
$\pi_p^k \in \mathbb{P}^k$ Paths from each node k to the slack
$\eta_{\pi_p^k} \subset \mathbb{N}$ Set of nodes that, for each node k, belong to path π_p^k that connects node k to the slack
$\beta_{\pi_p^k} \subset \mathbb{B}$ Set of branches that, for each node k, belong to path π_p^k that connects node k to the slack
$n \in \mathbb{S}$ Intersecting planes for current magnitudes linearization

Parameters

$\tilde{\boldsymbol{S}}_{k,t}^{D}$ Complex power absorbed at node k at time t [pu]
$\tilde{\boldsymbol{S}}_{g,t}^{G}$ Complex power injected by generator g at time t [pu]
$\tilde{\boldsymbol{V}}^{PS}$ Voltages of the slack nodes (HV nodes of primary substation) [pu]
$\tilde{\boldsymbol{V}}_{k,t}^{0}$ Initial value of node k voltage at time t [pu]
$\tilde{\boldsymbol{Y}}_{j}^{SH}$ Shunt admittance of branch j [pu]
$\tilde{\boldsymbol{Z}}_{j}$ Series impedance of branch j [pu]
$\tilde{\epsilon}^{\Delta V}$ Maximum amplitude of rapid voltage change [pu]
$\tilde{\rho}_j$ Probability of fault of branch j [-]
$\tilde{\Theta}$ User-defined angle range for voltage linearization [°]
$\tilde{A}_n/\tilde{B}_n/\tilde{C}_n$ Coefficients for branch current magnitudes linearization [pu]
$\tilde{F}$ Number of feeders [-]
$\tilde{I}_j^{MAX}$ Maximum current of branch j [A]
$\tilde{K}^{v}$ User-defined corrective factor for bus voltage linearization [pu]
$\tilde{M}$ Large value for Big-M technique [-]
$\tilde{N}_p^k$ Number of branches in path p for node k [-]
$\tilde{P}_{k,t}^{D}$ Real power absorbed at node k at time t [pu]
$\tilde{P}_{g,t}^{G}$ Real power injected by generator g at time t [pu]
$\tilde{V}_k^{MAX}$ Maximum voltage at node k [pu]
$\tilde{V}_k^{min}$ Minimum voltage at node k [pu]

Continuous variables

$\boldsymbol{I}_{j,t}$ Complex current flowing in branch j at time t [pu]
$\boldsymbol{I}_{j,k,t}^{+}$ Complex current flowing in branch j exiting from node k at time t [pu]
$\boldsymbol{I}_{j,k,t}^{-}$ Complex current flowing in branch j entering to node k at time t [pu]
$\boldsymbol{I}_{j,t}^{S}$ Complex current flowing in the series impedance of branch j at time t [pu]
$\boldsymbol{I}_{j,k,t}^{SH}$ Complex current flowing in the shunt admittance of branch j at node k side at time t [pu]
$\boldsymbol{I}_{g,t}^{G}$ Complex current injected by generator g at time t [pu]
$\boldsymbol{I}_{k,t}^{D}$ Complex current absorbed by demand at node k at time t [pu]
$i_{j,t}^{re}$ Real part of branch j current at time t [pu]
$i_{k,t}^{im}$ Imaginary part of branch j current at time t [pu]
$I_{j,t}^{approx}$ Approximation of branch j current magnitude at time t [pu]
$I_t^{0,avg}$ Average current flowing in $\mathbb{B}^0$ branches at time t [pu]
$I_t^{0,approx,avg}$ Approximation of the average current flowing in $\mathbb{B}^0$ branches at time t [pu]
$\boldsymbol{V}_{k,t}$ Complex voltage of node k at time t [pu]
$\Delta\boldsymbol{V}_{j,t}^{S}$ Auxiliary complex variable to ensure convergence related to the series impedance of branch j at time t [pu]
$\Delta\boldsymbol{V}_{j,t}^{SH}$ Auxiliary complex variable to ensure convergence related to the shunt admittance of branch j at time t [pu]
$v_{k,t}^{re}$ Real part of voltage at node k at time t [pu]
$v_{k,t}^{im}$ Imaginary part of voltage at node k at time t [pu]
$\delta_{k,t}$ Voltage angle of node k at time t [°]
$OF_{\#1}$ First objective function [-]
$OF_{\#2}$ Second objective function [-]
$\Omega_{j,t}$ Approximation of $OF_{\#1}$ [-]

Binary variables

$\sigma_{j,t}$ Status of branch j at time t
$\sigma_{j,t}^{C}$ Closing maneuver of branch j at time t
$\sigma_{j,t}^{O}$ Opening maneuver of branch j at time t
$W_{p,t}^{k}$ Status of path π_p^k connecting node k to the slack

(EVs), is playing an increasingly significant role in shaping energy demand profiles [8]. EVs are not only end-users of electricity but can also contribute to grid flexibility through vehicle-to-grid (V2G) technologies and smart charging solutions [9]; as highlighted in recent works, their integration offers promising opportunities for demand-side management and peak load reduction [10]. To effectively manage the challenges of fluctuating generation and evolving consumption patterns, Battery Energy Storage Systems (BESS) are being widely used at various voltage levels [11]. BESS provide critical services such as frequency regulation, load leveling, and energy arbitrage, supporting the stability and reliability of the grid [12]. Several recent studies emphasize their importance in mitigating RES variability and enhancing the resilience of distribution networks (DNs) [13]. Consequently, the electricity industry is shifting from passive DNs to active networks capable of dynamically responding to fluctuations in generation and consumption [14], and, in this context, the role of the Distribution System Operators (DSOs) will become essential.

Increased operational efficiency of DNs and optimized penetration of clean energy in DNs can be achieved, among other solutions, through short-term optimal reconfiguration [15], which adjusts network topology to withstand variations in load and generation [16]. This has to be coupled with a good monitoring of the grid for optimal real-time operation [17], which leads to investment in measurement equipment and development of algorithms for state estimation [18]. The study of optimal reconfiguration of DNs has gained significant importance in recent years due to its strategic usefulness in improving grid reliability and resilience [19]. In particular, this problem plays a crucial role in the post-fault restoration process, where the goal is to isolate the faulty sections of the DN and restore service to as many consumers as possible [20]. Reconfiguration techniques involve the opening and closing of circuit breakers and tie switches to modify the DN topology by following a specific objective function; as far as authors know, the common practice found in the bibliography review is to not consider such maneuvers directly. This approach can lead to results that are not feasible from a practical point of view and, therefore, should be overcome; hence, the goal of this article is to propose a reconfiguration algorithm for DN while considering the configuration shift steps [21].

1.2. Bibliography review

A summary of the bibliographic review performed on the DN reconfiguration problem and its main characteristics can be found in Table 1; the purpose of this subsection is to present the analysis performed.

Concerning the type of algorithm exploited, various methodologies have been proposed in the literature, ranging from classical optimization approaches to heuristic and metaheuristic algorithms, each addressing different aspects of the trade-offs between computational efficiency and solution accuracy [42]. The most important are:

- Metaheuristic methods have the advantage of being easy to model and do not require specific knowledge of mathematical assumptions about the problem; however, unlike deterministic methods, they can provide approximate results that are difficult to reproduce, and are less robust and accurate. They include techniques such as genetic algorithms [22], fuzzy multi-objective optimization [23,26], and Artificial Ecosystem-based Optimization [27].
- Mixed-Integer Nonlinear Programming (MINLP) models allow the integration of both discrete decision variables and nonlinear constraints and objectives. This formulation enables a more accurate mathematical representation of power system behaviors. Examples of MINLP-based approaches in the literature include [28] and [29]. However, especially in cases with high number of binary variables, MINLP can have high computational time, combined with the absence of guarantees for global optimality in large-scale applications.
- Recent advances in Mixed-Integer Linear Programming (MILP) solvers and their commercial availability are notable, primarily attributed to the integration of local search techniques and efficient heuristics designed to speed up the identification of initial feasible solutions [43]. They are based on the linearization of the constraints and objective functions while retaining the ability to handle integer variables; their main advantage is the possibility to obtain globally optimal solutions within controlled tolerances. MILP has been extensively adopted in the reviewed works, including [30–39].
- Lastly, some very recent studies are based on non-linear models implemented in Neural Networks [40] which, while very promising in terms of computational time and ability to easily deal with uncertainties, do not have the accuracy of deterministic models; moreover, they are dependent on training data characteristics, and therefore may not respond well if the actual data characteristics differ from the training data.

Despite the recent advances in stochastic and machine learning-based optimization techniques, MILP remains a suitable choice for DN reconfiguration due to its ability to deliver globally optimal solutions under a wide range of operational constraints. Unlike data-driven approaches, which depend heavily on training datasets, MILP guarantees repeatability and robustness. Moreover, compared to stochastic optimization (which typically requires extensive scenario generation and computational effort) MILP is more tractable for deterministic multi-period formulations and better suited to real-time or near real-time applications.

Concerning the objective functions in optimal reconfiguration, a large number of works focus on loss minimization, including [22–27,30–40], reflecting the priority of reducing operational costs and improving system efficiency [44]. Although it is an important goal [45], with the large increase in RES penetration, following this logic may not provide the stability or flexibility needed for their integration [46]. Hence, especially in recent years, new strategies have been developed, such as voltage deviation minimization [23,36], which targets the importance of keeping voltage profiles within acceptable bounds. Moreover, some models incorporate additional objectives such as load balancing, aimed at achieving a more uniform distribution of power flows [33,35,36], and hosting capacity, which quantifies the maximum level of distributed generation that can be integrated without compromising system constraints [29]; however, the proposed formulations balance the feeders by considering the power flows (not the currents) with respect to their maximum value and, therefore, assume the corresponding voltage value to be equal to the nominal one, thus leading to possible overestimates or underestimates of the actual values. Lastly, reliability is also considered in some models [26,27,36], highlighting the importance of improving system resilience. This last aspect is quantified by indices such as the SAIDI (the average duration of interruptions per user) and the SAIFI (the average number of times an interruption occurs per user) [47]; however, finding the information needed to calculate them, such as the probability of equipment failure, is not always easy.

Concerning the power flow (PF) model used, the reviewed studies adopt three main types of formulations: the Baran approximation, the polar representation, and the current-based rectangular model. The Baran formulation is an approximate power-based model originally proposed for radial DNs [41]; it simplifies the representation of PF

Table 1
Summary of the bibliography review on DN reconfiguration.

Reference	Type of algorithm	Objective function	PF formulation	Single/Multi period	Zero impedance	Transient shift time
[22]	Metaheuristic	Losses	Polar	Single	✗	✗
[23]	Metaheuristic	Losses, Voltage Deviation	Polar	Single	✗	✗
[24]	Metaheuristic	Losses	Polar	Single	✗	✗
[25]	Metaheuristic	Losses	Polar	Single	✗	✗
[26]	Metaheuristic	Losses, Reliability	Polar	Single	✗	✗
[27]	Metaheuristic	Losses, Reliability	Polar	Single	✗	✗
[28]	MINLP	Losses	Polar	Multi	✗	✓
[29]	MINLP	Hosting Capacity	Polar	Multi	✗	✗
[30]	MILP	Losses	Current-based rectangular	Single	✗	✗
[31]	MILP	Losses	Current-based rectangular	Single	✗	✗
[32]	MILP	Losses	Baran†	Single	✗	✗
[33]	MILP	Losses, Load Balancing	Baran†	Single	✗	✗
[34]	MILP	Losses	Baran†	Single	✗	✗
[35]	MILP	Losses, Load Balancing	Baran†	Single	✗	✗
[36]	MILP	Losses, Load Balancing Voltage Deviation, Reliability	Baran†	Single	✗	✗
[37]	MILP	Losses	Polar	Multi	✗	✗
[38]	MILP	Losses	Baran†	Single	✓	✗
[39]	MILP/Metaheuristic	Losses	Baran†	Single	✗	✗
[40]	Neural Network	Losses	Polar	Multi	✗	✗

† The Baran formulation is a power-based model described in [41].

equations, enabling efficient integration into optimization frameworks. This formulation is adopted in [32–36,38,39] and remains popular due to its tractability, particularly in MILP-based models. However, most of the constraints are based on power flows evaluated at the nominal voltage value, leading, as stated before, to possible inaccuracies. The polar formulation expresses voltages and currents directly through their magnitude and angle; it is used in [22–29,37,40]. This approach maintains a more direct link to the nonlinear nature of AC PF compared to power-based approximations, and therefore, is mainly used in metaheuristics, MINLP, and neural network models. Finally, the current-based rectangular formulation is employed in [30,31], where voltage and current phasors are expressed using real and imaginary components. This formulation provides a linear structure for certain applications (such as DN studies) but may be less accurate in highly meshed systems, such as Transmission Networks.

Another important aspect in the DN reconfiguration problem is the explicit consideration of breakers, since they need to be represented as zero-impedance branches. Almost all of the articles analyzed do not consider these components in the formulation, with the exception of Ref. [38], where, however, they are approximated as low impedances, an approach that can lead to problems with convergence of the algorithm due to unrealistic voltage drops in simulation or ill-conditioned system matrices [48]. This very last aspect is especially found in the traditional formulation of PF equations in polar coordinates, since inserting a component with zero or very small impedance would result in infinite admittance in the Y matrix. This drawback is addressed in the literature in efficient way for PF computation [49] and the state estimation problem [50]; however, these formulations are highly non-linear, which makes them difficult to include in a reconfiguration problem.

Lastly, most models adopt a single-period formulation, representing system conditions at a given time snapshot. This is appropriate for applications such as static reconfiguration or initial sizing studies. However, time-dependent phenomena—such as daily load variations, generation intermittency, or storage dynamics—require multi-period modeling, as done in [28,29,37,40]. Among these works, only [28] considers the actual number of maneuvers during reconfiguration, limited, however, to only minimizing them to achieve a given optimal configuration, thus ignoring possible dynamic constraints between maneuvers.

To summarize, the main criticalities found in the literature analysis are:

- Most studies focus on a single-time interval optimization (e.g., 1 h), while, from the point of view of normal operation, it is realistic to calculate an optimal network configuration applied over a multi-period time horizon to reduce the number of maneuvers and avoid excessive mechanical stress [51].
- The explicit consideration of breakers in MILP models is very challenging, as they need to be represented as zero-impedance branches. To the authors' knowledge, a robust model for zero impedance branches suitable for these applications is yet to be proposed. This aspect is of primary importance, both to consider the actual structure of primary/secondary substations (PS/SS) and their possible reconfiguration in the presence of multi-bar systems, and to represent the realistic possibility of a cable being opened only at one side, with the other remaining connected, the cable thus producing reactive power.
- While there is a large availability of algorithms for optimizing the network configuration, there remains a gap in optimizing the sequence and the number of maneuvers to securely move the network from an initial topology to the optimal one. This is a critical point as, in real-life, the number of maneuvers that can be applied is strongly constrained
  - by the number of available operators that can manually perform them;
  - by the low level of grid automation (few branches can be controlled remotely);
  - by security reasons, as a fault during the transit period can leave the DN in critical conditions. Hence, an optimal configuration that does not consider the transit period can be an unfeasible solution in practice.

1.3. Paper contribution

This work explicitly addresses the above-mentioned gaps by introducing several novel contributions:

(1) First, it proposes a reconfiguration algorithm that determines both the optimal final configuration of the distribution network and the optimal transition path—defined as a sequence and number of feasible switching operations (each consisting of a breaker closure followed by a breaker opening) that maintain radiality and full connectivity throughout the reconfiguration process. The optimization accounts for multi-period generation and load profiles, ensuring that all intermediate and final configurations satisfy network security constraints.
(2) Second, the model incorporates the Rapid Voltage Change (RVC) restriction, which represents a rapid lowering of the RMS value of the nodal voltage during switching maneuvers [52], an aspect overlooked in existing works. This allows for a more realistic assessment of transient disturbances during reconfiguration.
(3) Lastly, this work introduces a novel and computationally efficient method to model zero-impedance branches by embedding breakers directly into the optimization framework. The proposed approach avoids common numerical instability issues associated with ideal switch representations, while preserving model simplicity and robustness.

The rest of the paper is organized as follows: Section 2 illustrates the structure of the proposed methodology, Section 3 describes the complete model as a MINLP, Section 4 presents the proposed MILP formulation as an efficient linearization of MINLP, Section 5 summarizes the input data identification and the simulation results. Lastly, Section 6 highlights the conclusions.

2. Overview of the proposed methodology

This section presents the structure of the proposed algorithm, which will be described in Sections 3 and 4; the graphical representation is depicted in Fig. 1. In the upper part on the horizontal axis there is the time, while on the vertical axis the power produced/absorbed by the generators/loads of the grid for the entire time studied; the horizontal axis is divided to define the different time intervals (periods) that characterize the algorithm. In the lower part of the picture, on the other hand, a further subdivision of the time intervals (which will be described later) and the steps for switching from one configuration to another are represented.

The procedure starts from the initial configuration (CONFIG A) and the goal is to determine a new one (CONFIG B), optimal according to a defined objective and valid for a subsequent time horizon (OPERATIONAL TIME → $\mathbb{T}^{op}$), for which the load and generation profiles are known. To achieve this, it is necessary to define how early before OPERATIONAL TIME to start the shift process from CONFIG A to CONFIG B, i.e., to define the SHIFT TIME → $\mathbb{T}^{s}$. Within this time window, switching maneuvers are applied sequentially to move between the two configurations. Their number is limited due to various factors:

(1) to keep nodes connectivity and the radiality of the grid and minimize security risks (unexpected faults during the shift period risk leaving the DN in a critical state), the switches must be executed one at a time in an alternating $Close(C) - Open(O) - C - O - \cdots - O$ sequence, known as a feasible switch sequence [53];

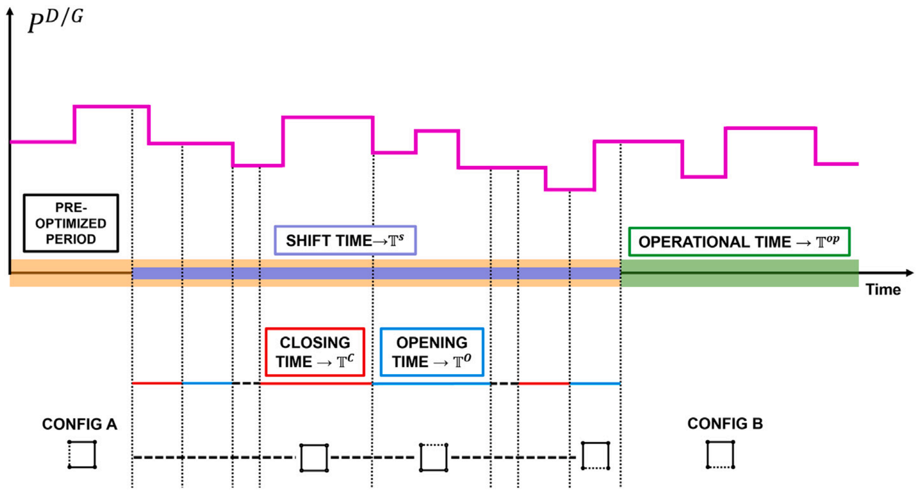

Fig. 1. Overview of the proposed methodology.

(2) the execution time of a feasible switch which can be slower if done manually by on field human intervention, or faster, if it can be activated by remote control, using proper communication systems - this last case can be rare given the poor automation level in current DNs.

These factors, combined, will determine the maximum number of feasible switches. Based on the objective function and due to the technical constraints of the DN (current and voltage limits, RVC), it is possible that the actual number of maneuvers is less than the maximum number.

To implement the feasible switches during SHIFT TIME, the DSO must first define an average time necessary to perform a maneuver; secondly, since load and generation power profiles are usually given over a discrete time interval (typically, 15 minutes) which is larger than the maneuver execution time (few minutes [54]), the power profile time interval is divided into several discrete sub-intervals during which the maneuvers can actually be performed. Fig. 2 illustrates this situation, where the orange intervals represent the discrete time intervals of power profiles while the purple time intervals are time intervals to perform switching maneuvers. The latter are evenly split into the alternating sequence of CLOSING TIME → $\mathbb{T}^c$ and OPENING TIME → $\mathbb{T}^o$ intervals, during which closing and opening maneuvers, respectively, can be performed to transit from the initial (CONFIG A) to the final optimized (CONFIG B) configuration.

As explained, the proposed model covers a base situation where at a certain point in time only one feasible switch can be performed either manually by a working team or automatically through remote control. If conditions to perform simultaneously more feasible switches are met (like more than one working team being available) then this representation can be used by properly reducing the average time necessary to perform a maneuver, e.g., by linking it to the number of working teams, and the maneuvers' times are placed under the same power level. Moreover, the dead time necessary for the working teams to move from one place to another can be easily modeled as the minimum shut-down time constraints in the traditional Unit Commitment problem [55] applied to the variables modeling the branches' status; as this technique is well known and can be easily implemented, this aspect was not considered in this work.

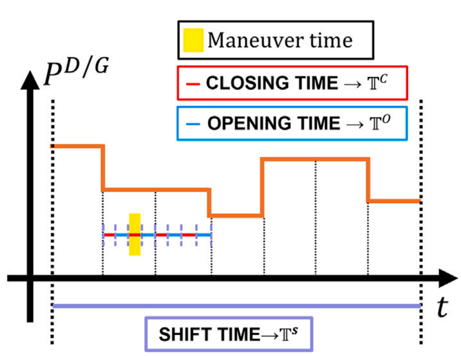

Fig. 2. SHIFT TIME definition procedure.

To summarize, the algorithm determines (1) the new optimized configuration (CONFIG B), obtained by maximizing an objective function that is subjected to network technical constraints over the OPERATIONAL TIME, and (2) the optimal steps, defined during SHIFT TIME, to switch between the two configurations while respecting network technical constraints. The link between the SHIFT TIME and OPERATIONAL TIME can be achieved by imposing a continuity condition that the branch statuses in OPERATIONAL TIME are equal to those in the last time interval of the SHIFT TIME.

3. Complete MINLP model

To clearly understand the proposed algorithm, first the adopted radiality model, which provides the structural basis necessary to effectively define and apply the objective functions, will be presented. Then, the objective functions and the remaining constraints will be explained.

3.1. The radiality model

The simplest way to model the topology of an electrical network is through the branch-to-node incidence matrix. In a meshed network with N nodes, a well-known theorem states that a set of N-1 branches forms a spanning tree (i.e., a connected graph using all vertices in which there are no loops [56]) if the corresponding columns of the incidence matrix form a full-rank submatrix [57]; however, applying this theorem in practice requires converting the matrix to row echelon form or calculating a determinant, both of which can be time-consuming for real-size systems. Therefore, to ensure the radiality and connectivity constraints, the model described in [39] has been adopted; the main properties are resumed in this subsection.

For a meshed network (here, a DN with all breakers closed), there are several alternative paths connecting a given bus to the PS, while for a normal operating condition in radial configuration, each bus is connected to the PS by a single unique path.

Let $\mathbb{P}^k$ be the set of paths associated with each node k:

$$\mathbb{P}^k = \{\pi_1^k, \pi_2^k, \dots, \pi_p^k, \dots, \pi_{np}^k\} \tag{1}$$

where each path π_p^k is a set of elements (nodes and branches) connecting node k to the PS and np is the total number of possible paths connecting node k to the PS. Moreover, let us define sets $\beta_{\pi_p^k}$ as the set of branches that belong to path π_p^k and the sets $\eta_{\pi_p^k}$ as the set of nodes that belong to path π_p^k. We can thus say that $\pi_p^k = \{\beta_{\pi_p^k}, \eta_{\pi_p^k}\}$.

Any radial network is characterized by only one of the paths in (1) being active (all branches in the path are connected) for each node k; hence, since the status of each path π_p^k must be represented, the following binary variable is defined:

$$W_{p,t}^k = \begin{cases} 1 & \text{if } \pi_p^k \text{ is the active path for bus } k \text{ at time } t \\ 0 & \text{otherwise} \end{cases} \tag{2}$$

Moreover, branch j status defined by the binary variable $\sigma_{j,t}$ can be expressed as:

$$\sigma_{j,t} = \begin{cases} 1 & \text{if branch } j \text{ is connected at time } t \\ 0 & \text{otherwise} \end{cases} \tag{3}$$

A candidate sub-network is both connected and radial if the following constraints are satisfied during $\mathbb{T}^o$ time intervals:

- each node has one active path only:

$$\sum_{p \in \mathbb{P}^k} W_{p,t}^k = 1, \forall k \in \mathbb{N}^\nabla \ \& \ \forall t \in \mathbb{T}^o \tag{4}$$

- if a path is active, all the branches belonging to the path must be connected:

$$\tilde{N}_p^k W_{p,t}^k \leq \sum_{j \in \beta_{\pi_p^k}} \sigma_{j,t}, \forall k \in \mathbb{N}^\nabla \ \& \ \forall t \in \mathbb{T}^o \tag{5}$$

- if a path is not active, at least one branch within the path must be opened:

$$(\tilde{N}_p^k - 1)(1 - W_{p,t}^k) \geq \sum_{j \in \beta_{\pi_p^k}} \sigma_{j,t}, \forall k \in \mathbb{N}^\nabla \ \& \ \forall t \in \mathbb{T}^o \tag{6}$$

For a clearer understanding of the above model, Fig. 3 shows an illustrative example: for the generic node k two possible paths exist, π_1^k and π_2^k. Set $\beta_{\pi_1^k}$ includes branches $(1)-(2)-(3)-(4)$, while set $\beta_{\pi_2^k}$ includes branches $(5)-(6)-(7)$. Sets $\eta_{\pi_1^k}$ and $\eta_{\pi_2^k}$, which represent the list of nodes that, for bus k, belong to path π_1^k and π_2^k respectively, include nodes $[1]-[2]-[3]$ and $[4]-[5]$ respectively.

For time t, if π_1^k is active, then $W_{\pi_1^k,t}^k = 1$ and, since $\tilde{N}_{\pi_1^k}^k = 4$, as per (5) $\sigma_1 = \sigma_2 = \sigma_3 = \sigma_4 = 1$. Then, since (4) forces π_2^k to not be active, $W_{\pi_2^k,t}^k = 0$ and, based on (6), $\sum_{j=4,5,6} \sigma_j \leq 2$, since $\tilde{N}_{\pi_2^k}^k = 3$, which implies that at least one of the branches of π_2^k is opened. Opposite constraints must be fulfilled if path π_2^k is the active one.

Constraints (4)–(6) are written only for $t \in \mathbb{T}^o$ since during the closing stages ($\mathbb{T}^c$) the network will necessarily have to be meshed and therefore the concept of "single active path" loses its meaning; moreover, during OPERATIONAL TIME ($\mathbb{T}^{op}$) the branch status is fixed to that of the last $\mathbb{T}^o$ time step and so constraints (4)–(6) are not necessary, as they are implicitly satisfied. This approach allows fewer equations to be processed, resulting in less computational time.

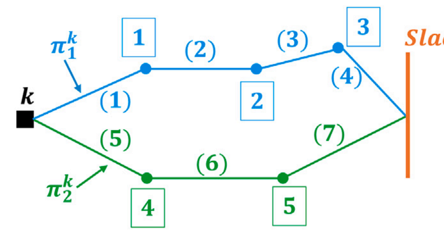

Fig. 3. Example of paths definition for node k.

3.2. Objective function

The goal of the proposed algorithm is to define the optimal configuration of a DN based on multi-period generation and load profiles while respecting the network constraints. Going beyond the traditional strategy for network reconfiguration, the losses minimization, in this study improvements are proposed on two promising objective functions found in the literature:

(1) *Feeder balancing*: a balanced distribution of the DN loading between the feeders can help in avoiding overloads (with a general improvement in the network efficiency) and guarantees a higher hosting capacity of the network, with the consequent efficient utilization of RES [58]. The first objective function can be expressed as:

$$OF_{\#1} = \min \sum_{\substack{j \in \mathbb{B}^0 \\ t \in \mathbb{T}^{op}}} \left| \frac{I_{j,t}}{\tilde{I}_j^{MAX}} - I_t^{0,avg} \right| \tag{7}$$

where, by assuming a DN with $\tilde{F}$ feeders,

$$I_t^{0,avg} = \frac{1}{\tilde{F}} \sum_{j \in \mathbb{B}^0} \frac{I_{j,t}}{\tilde{I}_j^{MAX}}, \forall t \in \mathbb{T}^{op} \tag{8}$$

With this objective function, the algorithm configures the network by trying to balance the loading of the various available feeders; the function minimizes the deviation between the loading of a given feeder and the average loading across all feeders.

(2) *Security of supply maximization*: this objective function aims at increasing the reliability of the DN by minimizing the impact of possible outages on the final customer. In an electric line, a failure can occur anywhere; without any information on the probability of failure, which can be hard to obtain in practice, it is reasonable to assume that a fault can occur anywhere along feeder length with same probability.

Hence, the longer a line is among the total length of the network, the higher the probability that a failure will occur on it. The probability of a fault occurring on line $\Lambda_{\hat{j}}$ is:

$$Pr(\Lambda_{\hat{j}}) = \frac{L_{\hat{j}}}{\sum_{j \in \mathbb{B}} L_j} = \tilde{\rho}_{\hat{j}} \tag{9}$$

Moreover, the greater the number of users connected to a given line, the greater the damage caused by the line possible disconnection. To quantify in a general manner this aspect, an example is first introduced: a simple grid, shown in Fig. 4, has two lines Λ_1 and Λ_2 of length L_1 and L_2, respectively, and two loads which withdraw a power P_1 and P_2, respectively. A fault in line Λ_1 causes the unavailability of loads P_1 and P_2, while a fault in line Λ_2 puts only P_2 out-of-service. Hence, the expected value of unsupplied

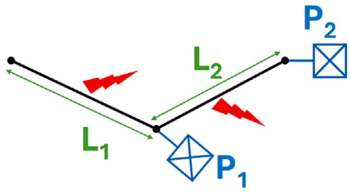

Fig. 4. Example of a system with two loads and two lines.

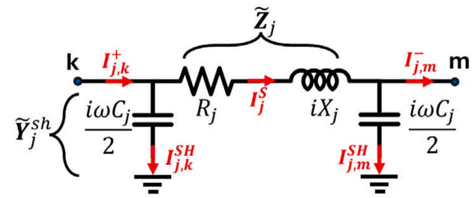

Fig. 5. Branch model adopted.

power due to faults in the considered grid is:

$$\Xi = \tilde{\rho}_1(P_1 + P_2) + \tilde{\rho}_2 P_2 = \tilde{\rho}_1 P_1 + (\tilde{\rho}_1 + \tilde{\rho}_2)P_2 \tag{10}$$

This can be generalized as:

$$\Xi = \sum_{\substack{k\in\mathbb{N}^\nabla\\ p\in\mathbb{P}^\mathbb{N}\\ t\in\mathbb{T}^{op}}} [W^k_{p,t} \sum_{j\in\beta_{\pi^k_p}} \tilde{\rho}_j \sum_{k\in\eta_{\pi^k_p}} \eta_{\pi^k_p}(\tilde{P}^D_{k,t} + \sum_{g\in\eta^\mathbb{G}} \tilde{P}^G_{g,t})] \tag{11}$$

Hence, the algorithm reconfigures the network by minimizing this expected value; in practical terms it distributes the most important users (thus those with higher power) as close to the PS as possible to reduce the impact of out-of-services due to unexpected faults. The second objective function can thus be expressed as:

$$OF_{\#2} = \min\ \Xi \tag{12}$$

From a practical point of view, the two objective functions (7) and (12) can be combined into a multi-objective approach and the resulting multi-objective model can then be solved through, for example, the well known techniques described in [59]. Since the goal of this study is to understand the behavior of these new objective functions individually, the multi-objective formulation approach is outside the scope of the article.

3.3. Power flow model

The traditional non-linear AC PF model in polar coordinates is not suitable for handling zero-impedance branches since inserting a component with zero or very small impedance would result in infinite admittance in the Y matrix; on the other hand, the so-called Current-Injection PF formulation [60,61] expressed in rectangular form[1] can overcome this issue, as will be shown.

The branch model used is illustrated in Fig. 5, where the generic branch j is represented (the real part of the shunt parameters of the lines has been assumed to be negligible).

Eq. (13) represents the Kirchhoff's current law at node k which links currents injected by the generators (defined over the set $\mathbb{G}$) and withdrawn by the loads with the currents entering into (defined by the set $\mathbb{B}^-_k$) and exiting from (defined by the set $\mathbb{B}^+_k$) the node through the branches of the grid:

$$\sum_{g\in\eta^\mathbb{G}} \boldsymbol{I}^G_{g,t} - \boldsymbol{I}^D_{k,t} = \sum_{j\in\mathbb{B}^+_k} \boldsymbol{I}^+_{j,t} - \sum_{j\in\mathbb{B}^-_k} \boldsymbol{I}^-_{j,t}, \forall k \in \mathbb{N} \tag{13}$$

Eqs. (14) and (15) represent the Ohm's law for the series and shunt parts of the branch, characterized by the series impedances $\tilde{\boldsymbol{Z}}_j$ and shunt admittances $\tilde{\boldsymbol{Y}}^{SH}_j$, respectively:

$$\boldsymbol{V}_{k,t} - \boldsymbol{V}_{m,t} = \tilde{\boldsymbol{Z}}_j \boldsymbol{I}^S_{j,t} + \Delta\boldsymbol{V}^S_{j,t}, \forall j \in \mathbb{B}\backslash\mathbb{B}^{Z_0} \tag{14}$$

$$\boldsymbol{I}^{SH}_{j,k,t} = \tilde{\boldsymbol{Y}}^{SH}_j \boldsymbol{V}_{k,t} + \Delta\boldsymbol{V}^{SH}_{j,t}, \forall j \in \mathbb{B}\backslash\mathbb{B}^{Z_0} \tag{15}$$

where $\Delta\boldsymbol{V}^S_{j,t}$ and $\Delta\boldsymbol{V}^{SH}_{j,t}$ are auxiliary variables necessary to ensure the convergence of the algorithm when the associated branch is opened. Through (16) and (17) they are null when branch j is connected at time t and equal to the voltage difference between unconnected busses when open (here the Big-M technique [62] is used and $\tilde{M}$ is a high enough value so that the values of these variables are not constrained).

$$-\tilde{M}(1-\sigma_{j,t}) \le \Delta\boldsymbol{V}^S_{j,t} \le \tilde{M}(1-\sigma_{j,t}), \forall j \in \mathbb{B}\backslash\mathbb{B}^{Z_0} \tag{16}$$

$$-\tilde{M}(1-\sigma_{j,t}) \le \Delta\boldsymbol{V}^{SH}_{j,t} \le \tilde{M}(1-\sigma_{j,t}), \forall j \in \mathbb{B}\backslash\mathbb{B}^{Z_0} \tag{17}$$

Eqs. (18) and (19) link the exiting and entering currents as shown in Fig. 5.

$$\boldsymbol{I}^+_{j,k,t} = \boldsymbol{I}^S_{j,t} + \boldsymbol{I}^{SH}_{j,k,t}, \forall j \in \mathbb{B} \tag{18}$$

$$\boldsymbol{I}^-_{j,m,t} = \boldsymbol{I}^S_{j,t} - \boldsymbol{I}^{SH}_{j,m,t}, \forall j \in \mathbb{B} \tag{19}$$

Eq. (20) sets, to correctly solve the PF problem, the voltage at the PS, $\tilde{V}^{PS}$, to a fixed value:

$$\boldsymbol{V}_{k,t} = \tilde{\boldsymbol{V}}^{PS}, \forall k \in \mathbb{N}\backslash\mathbb{N}^\nabla \tag{20}$$

Constraints (21) and (22) are the formulas for the complex power withdrawn by demands $\tilde{\boldsymbol{S}}^D_{k,t}$ and injected by generators $\tilde{\boldsymbol{S}}^G_{g,t}$; they link the power generation and demand profiles to the voltage and current variables:

$$\tilde{\boldsymbol{S}}^D_{k,t} = \boldsymbol{V}_{k,t}\boldsymbol{I}^{D*}_{k,t}, \forall k \in \mathbb{N} \tag{21}$$

$$\tilde{\boldsymbol{S}}^G_{g,t} = \boldsymbol{V}_{k,t}\boldsymbol{I}^{G*}_{g,t}, \forall k \in \mathbb{N} \tag{22}$$

Eq. (23) forces the currents to be zero if the branches are opened, and smaller than the maximum current $\tilde{I}^{MAX}_j$ if connected:

$$|\boldsymbol{I}^+_{j,t}| \le \tilde{I}^{MAX}_j \sigma_{j,t}, \forall j \in \mathbb{B} \tag{23}$$

Lastly, (24) limits the bus voltages between their lower and upper limits, $\tilde{V}^{min}_k$ and $\tilde{V}^{MAX}_k$:

$$\tilde{V}^{min}_k \le |\boldsymbol{V}_{k,t}| \le \tilde{V}^{MAX}_k, \forall k \in \mathbb{N}^\nabla \tag{24}$$

3.4. Zero-impedance breaker model

The current-based formulation can accurately model breakers as zero-impedance branches. Their main property is that the voltages at the two ends are equal as long as the breaker is closed and carries current. While (14)–(17) are written only for non-zero-impedance branches, for the breakers the following constraints are defined according to the structure in Fig. 6:

$$-\tilde{M}(1-\sigma_{j,t}) \le \boldsymbol{V}_{k,t} - \boldsymbol{V}_{m,t} \le \tilde{M}(1-\sigma_{j,t}), \forall j \in \mathbb{B}^{Z_0} \tag{25}$$

$$\boldsymbol{I}^+_{conj,t} = \boldsymbol{I}^-_{conj,t}, \forall j \in \mathbb{B}^{Z_0} \tag{26}$$

Eq. (25) is blind if the breaker is open (so when $\sigma_{j,t}$ is zero) and no constraints on the voltage of the buses connected by the breaker are present; on the other hand, if the breaker is closed, it forces the two voltages to be equal, thus achieving the desired result. Finally, (26) forces the current entering the breaker to be equal to the current exiting the breaker; the latter is valid both when the breaker is closed and when it is open (in which case the two currents, as for (23), will be equal to zero).

[1] Henceforth, a bold symbol represents a complex number written in rectangular form (e.g. $\boldsymbol{D} = d^{re} + i \cdot d^{im}$, where $i = \sqrt{-1}$).

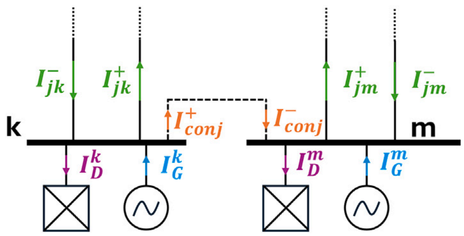

Fig. 6. Breaker model adopted.

3.5. Modeling of configuration shift steps

During the SHIFT TIME, the optimal steps to move from the initial configuration to the optimal one, while respecting the network's technical constraints, are defined; hence, all the following constraints are $\forall t \in \mathbb{T}^s$. Eq. (27) links the branch j status at time t to the previous time step $t-1$ through the closing and opening maneuvers, $\sigma_{j,t}^C$ and $\sigma_{j,t}^O$, respectively.

$$\sigma_{j,t} = \sigma_{j,t-1} + \sigma_{j,t}^C - \sigma_{j,t}^O \;\forall t \in \mathbb{T}^s \tag{27}$$

To avoid excessive mechanical stress on the equipment, which can lead to an early replacement of the breakers [37], each branch is allowed to change its status only once during the SHIFT TIME through (28), while (29) limits the maneuvers in each time step to at most one, according to the modeling of a feasible switch explained in Section 2.

$$\sum_{t\in\mathbb{T}^s} (\sigma_{j,t}^C + \sigma_{j,t}^O) \le 1 \tag{28}$$

$$\sum_{j\in\mathbb{B}} (\sigma_{j,t}^C + \sigma_{j,t}^O) \le 1, \forall t \in \mathbb{T}^s = \mathbb{T}^c \cup \mathbb{T}^o \tag{29}$$

Eqs. (30) and (31) prevent a closing maneuver during the opening time steps $\mathbb{T}^o$, and an opening maneuver during the closing time steps $\mathbb{T}^c$, respectively, guaranteeing the close-open alternation.

$$\sum_{j\in\mathbb{B}} \sigma_{j,t}^C \le 0, \forall t \in \mathbb{T}^o \tag{30}$$

$$\sum_{j\in\mathbb{B}} \sigma_{j,t}^O \le 0, \forall t \in \mathbb{T}^c \tag{31}$$

Lastly, (32) models the RVC limits as per [52]:

$$|\boldsymbol{V}_{k,t}| - |\boldsymbol{V}_{k,t-1}| \le \tilde{\epsilon}^{\Delta V}, \;\forall t \in \mathbb{T}^s \tag{32}$$

while (33) links the branch status during the OPERATIONAL TIME period with the one defined at the end of the SHIFT TIME:

$$\sigma_j = \sigma_{j,\tilde{t}_{end}} \tag{33}$$

where $\tilde{t}_{end}$ represents the last time interval of the SHIFT TIME period.

It is worth noting that the PF constraints (13)–(26) are written for $\forall t \in \mathbb{T}$, while during OPERATIONAL TIME there is only one σ_j constrained by (33) that substitutes $\sigma_{j,t}, \forall t \in \mathbb{T}^{op}$ in constraints (13)-(24); this formulation allows fewer equations to be processed and, consequently, reduces computational time. Moreover, to further reduce computation time, it is possible to define subsets of $\mathbb{N}^{\nabla}$ and $\mathbb{B}$ by following the procedure described in Appendix A and writing (23) and (24) for these subsets only.

4. Proposed MILP model

The optimization model made of $OF_{\#1}$ or $OF_{\#2}$ subjected to constraints (2)–(6), (8), (11), (13)–(33) is linear in its equations except for (7), (21), (22), (23), (24), and (32); the resulting optimization model is a large MINLP program which, by its nature, is difficult to solve in reasonable computation time. Hence, the linearization of the model is proposed in this Section and a numerically tractable MILP model is obtained, without losing the accuracy inherent to the MINLP model.

4.1. Linearization of branch current magnitudes

Branch current magnitudes in (23) are estimated using the approximation of the Euclidean norm proposed in [63] which is based on intersecting planes; for the sake of brevity, only the key points are reported. The approximated current magnitude $\Gamma_{j,t,n}$ is defined as:

$$\Gamma_{j,t,n} = \frac{i_{j,t}^{re}\tilde{A}_n + i_{j,t}^{im}\tilde{B}_n}{\tilde{C}_n}, \forall j \in \mathbb{B}, \forall t \in \mathbb{T}, \forall n \in \mathbb{S} \tag{34}$$

where n are the elements of the intersectional planes set $\mathbb{S}$ and $\tilde{A}_n$, $\tilde{B}_n$, $\tilde{C}_n$ are suitable parameters defined as for [64]. Once (34) has been introduced, (23) becomes:

$$\Gamma_{j,t,n} \le \tilde{I}_j^{MAX}\sigma_{j,t}, \forall j \in \mathbb{B}, \forall t \in \mathbb{T}, \forall n \in \mathbb{S} \tag{35}$$

4.2. Linearization of the absolute value in $OF_{\#1}$

Eq. (34) is not the actual value of the branch current magnitude, but it returns a value for each plane n that must satisfy (35). The approximated value of the current magnitude can be obtained as:

$$|\boldsymbol{I}_{j,t}^{+}| \approx max_{n\in\mathbb{S}}\{\Gamma_{j,t,n}\} \tag{36}$$

which can be linearized by introducing (37):

$$I_{j,t}^{approx} \ge \Gamma_{j,t,n} \tag{37}$$

and by minimizing the term $I_{j,t}^{approx}$ in the objective function, the value of $I_{j,t}^{approx}$ is pushed against the highest value of $\Gamma_{j,t,n}$, and condition (36) is thus achieved. Eq. (8) then becomes:

$$I_t^{0,approx,avg} = \frac{1}{\tilde{F}} \sum_{j\in\mathbb{B}^0} \frac{I_{j,t}^{approx}}{\tilde{I}_j^{MAX}}, \forall t \in \mathbb{T}^{op} \tag{38}$$

To linearize the absolute value in (7), variable $\Omega_{j,t}$ is defined as:

$$\Omega_{j,t} \ge \left(\frac{I_{j,t}^{approx}}{\tilde{I}_j^{MAX}} - I_t^{0,approx,avg}\right), \forall j \in \mathbb{B}^0 \;\&\; \forall t \in \mathbb{T}^{op} \tag{39}$$

$$\Omega_{j,t} \ge -\left(\frac{I_{j,t}^{approx}}{\tilde{I}_j^{MAX}} - I_t^{0,approx,avg}\right), \forall j \in \mathbb{B}^0 \;\&\; \forall t \in \mathbb{T}^{op} \tag{40}$$

and, by the same mechanism as in (36)–(37), the term $\Omega_{j,t}$ is minimized in the objective function.

Hence, the objective function (7) becomes:

$$OF_{\#1} = \min \sum_{\substack{j\in\mathbb{B}^0 \\ t\in\mathbb{T}^{op}}} \left(\Omega_{j,t} + I_{j,t}^{approx}\right) \tag{41}$$

4.3. Linearization of power injections

Linear expressions for (21) and (22) are obtained using first order approximations considering constant the real and imaginary values of bus voltages [63]:

$$\tilde{\boldsymbol{S}}_{k,t}^{D} \approx \tilde{\boldsymbol{V}}_{k,t}^{0}\boldsymbol{I}_{k,t}^{D*} \tag{42}$$

$$\tilde{\boldsymbol{S}}_{g,t}^{G} \approx \tilde{\boldsymbol{V}}_{k,t}^{0}\boldsymbol{I}_{k,t}^{G*} \tag{43}$$

The iterative procedure to define $\tilde{\boldsymbol{V}}_{k,t}^{0}$ is summarized in Fig. 7; initially, the estimated values can be selected from an AC-PF calculation, historical data, or flat start. Then the optimization is performed, and the obtained values of $v_{k,t}^{re}$ and $v_{k,t}^{im}$ are used to calculate $\boldsymbol{V}_{k,t}$; now convergence is checked by evaluating if $\left|\tilde{\boldsymbol{V}}_{k,t}^{0} - \boldsymbol{V}_{k,t}\right| \le \tilde{\epsilon}^{v}$. If yes, then the iterative procedure is stopped, otherwise $\tilde{\boldsymbol{V}}_{k,t}^{0}$ for the following iteration is updated by using the obtained value of $\boldsymbol{V}_{k,t}$, and the iterative procedure continues. Paper [63] shows that the initial approximation already provides a very good accuracy with respect to the AC PF results (≤ 2 %). Extended tests carried out by the authors show that 2–3 iterations are enough to reach real AC-PF level accuracy.

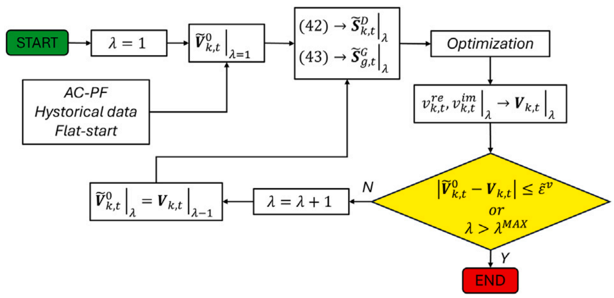

Fig. 7. Iterative procedure to define the linearization of power injections.

4.4. Linearization of bus voltage magnitudes

Eqs. (24) and (32) are linearized by assuming that, for a DN, voltage angles are small [65] and, consequently, the real part of voltage, $v^{re}_{k,t}$, is much higher than the imaginary one, $v^{im}_{k,t}$, which leads to the following approximation:

$$|\boldsymbol{V}_{k,t}| = |v^{re}_{k,t} + i \cdot v^{im}_{k,t}| \approx v^{re}_{k,t} \tag{44}$$

Eq. (44) represents a slight underestimation of $|\boldsymbol{V}_{k,t}|$, since, for every complex number,

$$v^{re}_{k,t} \leq |\boldsymbol{V}_{k,t}| \tag{45}$$

Therefore, the left-hand side of (24) can be rewritten without any problems for grid security (at most the lower voltage limit is slightly overestimated):

$$v^{re}_{k,t} \geq \tilde{V}^{min}_k \tag{46}$$

On the other hand, this is not true for the right-hand side of (24): based on (45), $v^{re}_{k,t} \leq \tilde{V}^{MAX}_k$ does not imply $|\boldsymbol{V}_{k,t}| \leq \tilde{V}^{MAX}_k$. To improve the approximation of (44), a corrective factor greater than one must be introduced. Since

$$v^{re}_{k,t} = \frac{\boldsymbol{V}_{k,t}}{cos(\delta_{k,t})} \tag{47}$$

ideally this factor should be equal to $\frac{1}{cos(\delta_{k,t})}$ but, being $\delta_{k,t}$ a variable, this introduces a ratio which must then be linearized. To overcome this issue, an angle range $\pm\tilde{\Theta}$ is introduced, which represents the maximum voltage angle possible in the DN under study. Once defined, the corrective scaling factor $\tilde{K}^v$ is evaluated as:

$$\tilde{K}^v = \frac{1}{\Re\{e^{i\cdot\tilde{\Theta}}\}} = \frac{1}{cos(\tilde{\Theta})} \tag{48}$$

Of course when the voltage angle $\delta_{k,t}$ is exactly $\pm\tilde{\Theta}$, then $\tilde{K}^v v^{re}_{k,t} = |\boldsymbol{V}_{k,t}|$; for $\delta_{k,t} \leq 45°$ we have that the smaller the angle, the greater the real part of the vector. Hence, for $\delta_{k,t} < \tilde{\Theta}$ we have that $\tilde{K}^v v^{re}_{k,t} > |\boldsymbol{V}_{k,t}|$. Therefore, the right-hand side of (24) becomes:

$$\tilde{K}^v v^{re}_{k,t} \leq \tilde{V}^{MAX}_k \tag{49}$$

To find the value of $\tilde{\Theta}$, it is reminded that voltage angles in an electric grid mainly depend on branch impedances and flowing currents (i.e., the net difference between the real generated power and the real absorbed power) [66]. In a reconfiguration study the structure of the DN is not fixed and, therefore, the impedances between the network buses are not known *a−priori*. However, it is reasonable to assume that network operators know which branches are controllable and which are not; therefore, the "worst possible condition" in terms of angles (i.e., the one that leads to having the highest value) can be studied and the results stored offline pre-optimization. On the other hand, with regard to users' profiles, perfect knowledge of them was assumed in this study for OPERATIONAL TIME intervals; however, this condition is not always possible (one possible cause is the low observability of actual DNs). Under these conditions, the correct determination of $\tilde{\Theta}$, which represents the evaluated upper limit of all the voltage angles in the DN, can be cumbersome; hence, the value can be chosen based on historical data or, for a more robust solution, based on literature analysis (for example, reference [31] states that in a DN voltage angles rarely go beyond 10°). It is nevertheless advisable to consider a higher $\tilde{\Theta}$ since, in any case, the introduction of $\tilde{K}^v$ leads to a slight overestimation of $|\boldsymbol{V}_{k,t}|$, and the approximation (49) remains on the safe side for grid security.

Following the same idea, (32) becomes:

$$\tilde{K}^v(v^{re}_{k,t} - v^{re}_{k,t-1}) \leq \tilde{\varepsilon}^{\Delta V} \tag{50}$$

5. Simulations and results

The model has been implemented in GAMS 38.3.0 and solved using CPLEX 12.6; the relative gap set-up is 0 %—this was done in order not to jeopardize the accuracy of the linearizations introduced in the MILP models. Simulations have been carried out with an Intel®Core™i9-10980XE CPU @ 3.00 GHz, 18 Cores, 36 Processors, RAM 64 GB PC.

5.1. Input data

Numerical tests have been carried out on the IEEE 12-bus system [67] and the IEEE 69-bus system [68] (for the latter branches were added to make the basic configuration meshed). The demand was defined for one day with a resolution of 60 minutes using the demand shapes of Ref. [69] properly rescaled and distributed randomly and uniformly across the nodes. Each demand has been equipped with Photovoltaic (PV) panels (with 14 % assumed efficiency) dimensioned to cover 60 % of the peak load using irradiation data from Ref. [70] related to Milan area for the day February 1st, 2020 (a representative winter day for the specified area). Simulations were carried out for the irradiation data of two consecutive summer days—August 14th and 15th, 2020 [70]—at 1:00 pm. It is worth noting that the proposed method assumes full knowledge of future generation and load profiles for the OPERATIONAL TIME period. While this assumption is acceptable for deterministic studies, it may not always hold in practical applications due to forecasting uncertainty or limited observability in DNs. However, future extensions of the proposed model could integrate robust or stochastic optimization techniques to explicitly account for profile uncertainty, without losing, in any case, the basic proposed formulation. As for [52], $\tilde{\varepsilon}^{\Delta V}$ has been set to 0.05; finally, assuming a maximum voltage angle $\tilde{\Theta} = 10°$ [31], $\tilde{K}^v = 1.0154$. Due to their unavailability, voltage bounds have been set equal to $V^{min}_k = 0.9$ and $V^{MAX}_k = 1.1$ [71].

5.2. Simulations on IEEE 12-bus system

The initial configuration for the IEEE 12 bus system is depicted in Fig. 8, where the black edges represent the connected lines, the black dotted edges represent the open branches, and the green star is the PS (slack node); the initial load, generation, and net real power profiles (which although similar in aggregate, are nodally different) are plotted in Fig. 9, where the green area represents the OPERATIONAL TIME period, while the violet one shows the hours preceding it, during which SHIFT TIME is defined. This small-sized DN is used to test the impact of the new modeling features: the objective function evaluation, the SHIFT TIME representation and the precise tie-line model.

5.2.1. Objective functions evaluation

The two objective functions for the OPERATIONAL TIME are evaluated considering the initial, not-optimal, configuration, leading to $OF^0_{\#1} = 3.9425$ and $OF^0_{\#2} = 0.88$; in particular the first value, which represents the level of unbalance of the network, mostly depends on the non-symmetrical initial configuration of the DN (see Fig. 8).

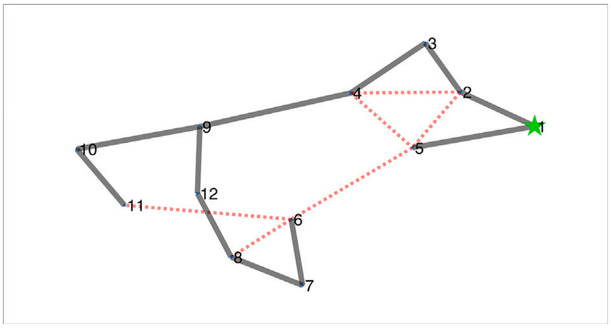

Fig. 8. IEEE 12-bus system: initial configuration.

Table 2
IEEE 12-bus system: ideal objective function values.

	$OF_{\#1}$	$OF_{\#2}$
min $OF_{\#1}$	**1.7839**	0.3571
min $OF_{\#2}$	1.8126	**0.3436**

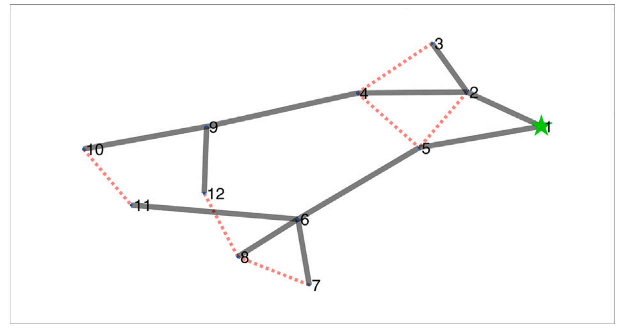

Fig. 10. IEEE 12-bus system: final configuration without considering the optimal steps evaluating $OF_{\#1}$.

First, the ideal optimum is calculated by assuming all maneuvers are performed simultaneously and just before the start of OPERATIONAL TIME to define the optimal configuration for OPERATIONAL TIME (this is achieved by neglecting SHIFT TIME corresponding constraints and optimizing directly OPERATIONAL TIME). The optimization algorithm is run considering separately both $OF_{\#1}$ and $OF_{\#2}$, and the obtained values are summarized in Table 2, where also the not optimized objective function values are shown. The corresponding ideal values are 215 % lower for $OF_{\#1}^{ideal}$ and 60 % lower for $OF_{\#2}^{ideal}$ with respect to the initial values.

Moreover, Table 2 shows that the not optimized values of the objective functions are close to their optimized values: when $OF_{\#1}$ is optimized $OF_{\#2}$ is 3.93 % higher than its optimal value, while when $OF_{\#2}$ is optimized $OF_{\#1}$ is 1.61 % higher than its optimal value. This is explained by the fact that, under specific conditions $OF_{\#2}$ is equivalent to $OF_{\#1}$: for equal branch lengths and equal nodal customer sizes branch failure probabilities are all equal and each node is equally at risk; minimizing $OF_{\#2}$ becomes balancing the feeders in terms of powers. The analyzed network is close to these ideal conditions: branches are very short and relatively equal in length, while the spread of nodal power values is small. In these conditions using $OF_{\#2}$ is the better choice as it explicitly models the security of supply.

As stated in Section 3, the two implemented objective functions can be studied together through multi-objective formulations, approach which, being well known, is not the subject of research in this article. However, the multi-objective formulation is of interest if the different objective functions studied turn out to be complementary (i.e., the maximization/minimization of one leads to the minimization/maximization of the other); as can be seen from the results reported in Table 2, the two objective functions are not found in this condition (the values obtained in the different evaluations are very similar to each other), which makes their study in multi-objective formulation not highly relevant.

Figs. 10 and 11 show the obtained ideal optimal configurations. It can be seen that the configurations are very similar. The only differences are the connections of nodes 8 and 11: by minimizing $OF_{\#2}$, the algorithm connects the most important loads as close to the slack as possible (to decrease the probability of being out-of-service), without checking the balance of feeders; nodes 8 and 11 have loads that, with the configuration of Fig. 11, have a smaller electrical distance from the balance, and, therefore, the algorithm chooses that particular connection. These observations validate the analysis of the previous paragraph.

5.2.2. SHIFT TIME evaluation

To test the impact of SHIFT TIME modeling, the number of time steps in $\mathbb{T}^s$ was set to 10, allowing maximum of 10 maneuvers, while the start of SHIFT TIME was set two hours before OPERATIONAL TIME start, therefore allowing up to five maneuvers per hour; hence, the SHIFT TIME steps measure 12 minutes each. Based on the results obtained in Section 5.2.1, $OF_{\#2}$ is studied here since it is the best choice in this case.

The sequence of the identified four maneuvers is summarized in Table 3; since the SHIFT TIME generation/load profile is almost constant

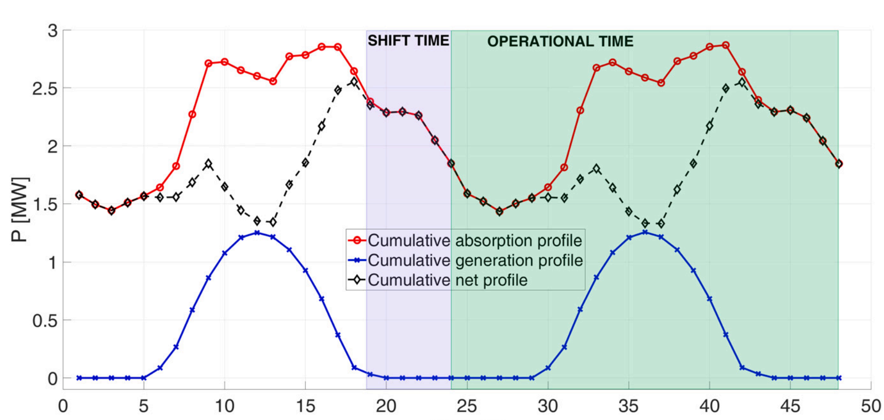

Fig. 9. IEEE 12-bus system: load, generation, and net real power profiles.

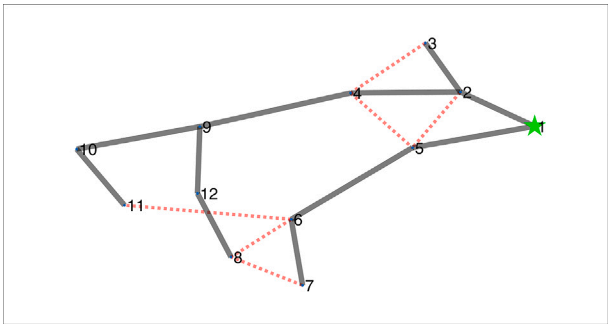

Fig. 11. IEEE 12-bus system: final configuration without considering the optimal steps evaluating $OF_{\#2}$.

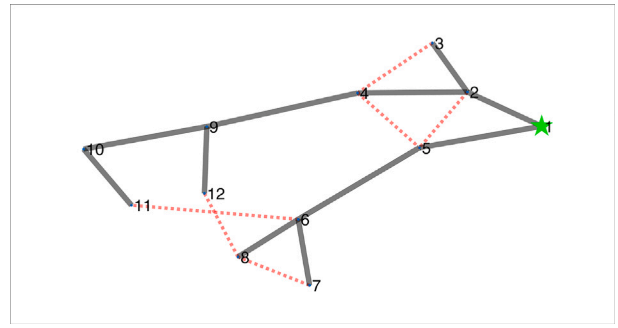

Fig. 13. IEEE 12-bus system: final configuration considering the optimal steps with $\tilde{\epsilon}^{\Delta V} = 0.01$.

Table 3
IEEE 12-bus system: sequence of the maneuvers.

t	Line	Operation
3	5–6	C
4	3–4	O
9	2–4	C
10	8–7	O

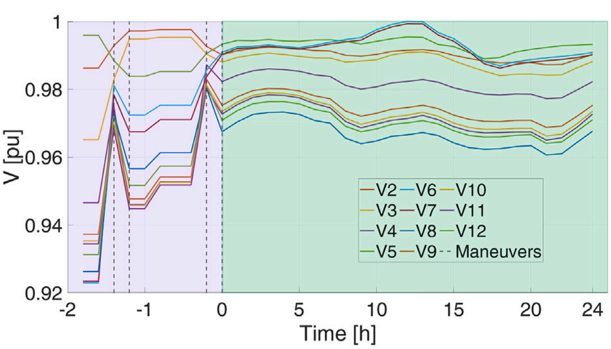

Fig. 12. IEEE 12-bus system: voltage trends during the maneuvers and the $\mathbb{T}^{op}$.

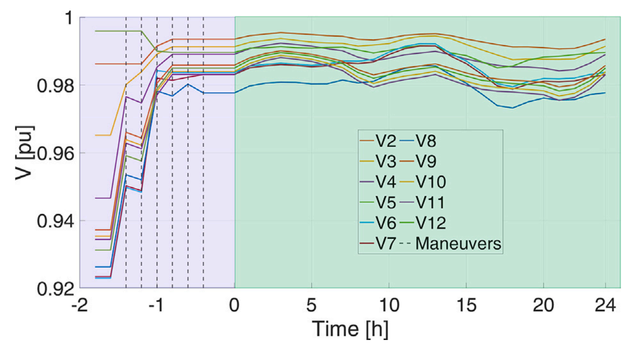

Fig. 14. IEEE 12-bus system: voltage trends during the maneuvers and the $\mathbb{T}^{op}$ with $\tilde{\epsilon}^{\Delta V} = 0.01$.

Table 4
IEEE 12-bus system: sequence of the maneuvers with $\tilde{\epsilon}^{\Delta V} = 0.01$.

t	Line	Operation
3	2–4	C
4	3–4	O
5	5–6	C
6	8–12	O
7	8–6	C
8	8–7	O

(see Fig. 9), the feasible switch execution times are mostly impacted by the network constraints. There are no currents close to limits recorded, thus the focus is on voltage constraints. Fig. 12 shows the voltage trends during $\mathbb{T}^s$ and $\mathbb{T}^{op}$ periods; it can be seen that voltage limits are well respected and, despite the large flicker of node 11 -around 0.03 pu-, the RVC constraint, which refers only to the nodal voltage lowering [52], is respected. Hence, no network constraints are activated and the obtained configuration coincides with the ideal one (see Fig. 11).

In these conditions (no current and voltage limits active), the only constraint with impact during SHIFT TIME remains the RVC constraint. This is evaluated by reducing $\tilde{\epsilon}^{\Delta V}$ from 0.05 to 0.01; this modification renders the open maneuver at $t = 4$ infeasible and, consequently, the first feasible switch. The new final configuration and voltage trends are shown in Figs. 13 and 14, respectively, while the new sequence of maneuvers is summarized in Table 4. Due to the tighter constraint on $\tilde{\epsilon}^{\Delta V}$, the algorithm performs 6 maneuvers, instead of 4, to arrive at the optimal configuration, and in this case $OF^1_{\#2} = 0.3449$, which is 0.13 % higher than the ideal one. This result highlights the importance of modeling the SHIFT TIME period in optimal reconfiguration problems, since not considering it explicitly could lead to better results regarding the final OPERATIONAL TIME configuration (i.e., $OF^{ideal}_{\#2}$), but this would then not be feasible to achieve in practice without risking network violation constraints during SHIFT TIME.

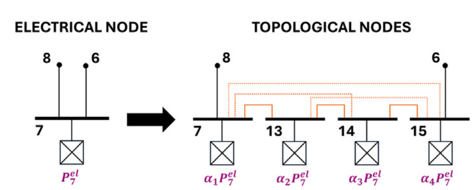

Fig. 15. IEEE 12-bus system: electrical node 7 and its equivalent topological one.

5.2.3. Bus-ties modeling evaluation

Lastly, the impact of modeling bus-ties is studied. The load profile in Fig. 9 previously used is modified by considering a large load at node 7 (i.e., 20 times larger than the initial one), which represents four independent demands connected to different topological nodes, but electrically the same (i.e. they are short-circuited through bus-ties). This is illustrated in Fig. 15, where split coefficients α_i are used to distribute the total electrical load P^{el}_7 to the topological nodes. They have been randomly set, so that $\alpha_1 = 0.3143$, $\alpha_2 = 0.0619$, $\alpha_3 = 0.1236$, and $\alpha_4 = 0.5002$ (their sum is 1).

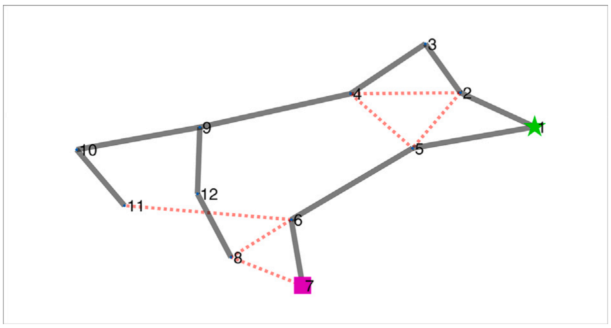

Fig. 16. IEEE 12-bus system: final configuration with additional demand and no bus-ties.

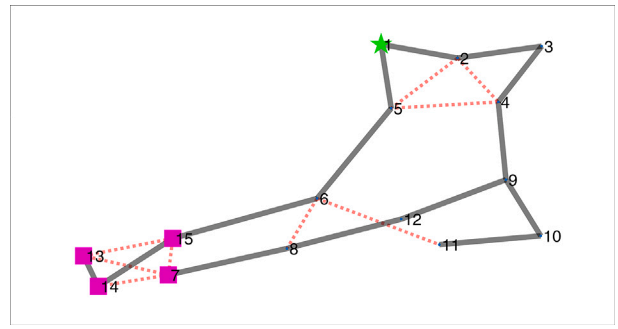

Fig. 18. IEEE 12-bus system: final configuration with additional demand and with bus-ties.

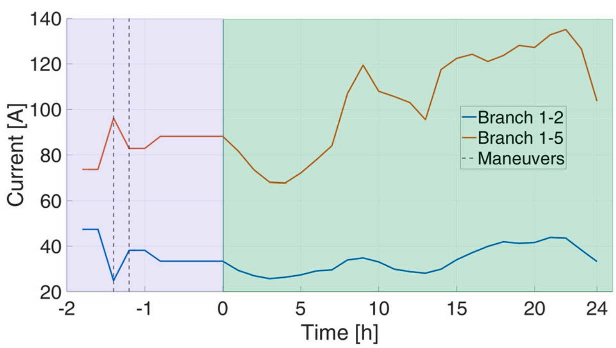

Fig. 17. IEEE 12-bus system: current trends in $\mathbb{B}^0$ branches during the maneuvers and the $\mathbb{T}^{op}$ with additional demand and no bus-ties.

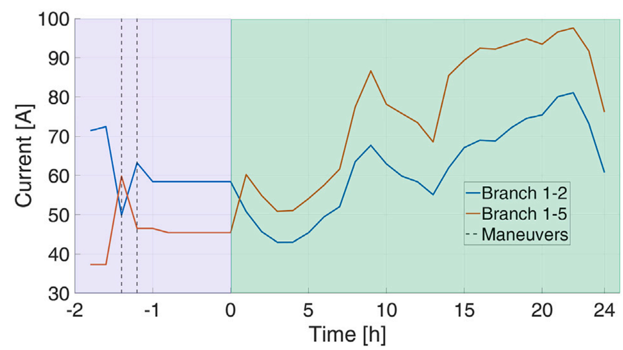

Fig. 19. IEEE 12-bus system: current trends in $\mathbb{B}^0$ branches during the maneuvers and the $\mathbb{T}^{op}$ with additional demand and with bus-ties.

Table 5
IEEE 12-bus system: sequence of the maneuvers with additional demand and no bus-ties.

t	Line	Operation
3	5–6	C
4	8–7	O

Table 6
IEEE 12-bus system: sequence of the maneuvers with additional demand and with bus-ties.

t	Line	Operation
3	5–6	C
4	7–13	O

Since the modeling of bus-ties has great impact on the circulating currents in the slack-connected branches, $OF_{\#1}$ was chosen for minimization this time. At first $OF_{\#1}$ has been evaluated by considering node 7 as a unique electrical node (i.e., the left-hand side of Fig. 15), therefore without considering bus-tie modeling and the possibility of splitting the connected load. The final configuration and the current magnitude trends of $\mathbb{B}^0$ branches are depicted in Fig. 16 (for which a maximum current $\tilde{I}_j^{MAX} = 160\ A$ was defined for both branches, in the absence of information) and Fig. 17, respectively. Table 5 summarizes the sequence of the maneuvers. It can be seen that the two feeders are not well balanced (since the additional load is entirely connected to the PS through branch $1-5$ only). In this case, $OF_{\#1} = 854.24$, a value that, represents the unbalance factor between the feeders (the lower this value, the more balanced $\mathbb{B}^0$ branches are). It is worth noting that connecting node 7 to the other feeder would shift the imbalance between the two feeders and, therefore, qualitatively the solution would not change. In conclusion, there is no possibility to balance the two feeders well due to the high value of the load at node 7.

Secondly, $OF_{\#1}$ is evaluated by considering the topological structure of node 7 (i.e. the right-hand side of Fig. 15), therefore by modeling the bus-ties and by allowing the split of the connected load through their maneuvers. The final configuration and the current magnitude trends of $\mathbb{B}^0$ branches are depicted in Figs. 18 and 19, respectively, while Table 6 summarizes the sequence of the maneuvers. In this case, the two branches are much better balanced with respect to the previous case since, now, the additional load is distributed between the two feeders (branches $1-2$ and $1-5$). With these assumptions, $OF_{\#1} = 186.37$, which is around 4.6 times lower than the previous one; this result demonstrates the importance of proper modeling of bus-ties (treated in this study as zero-impedance branches) as, in addition to a more accurate representation of the infrastructure, it allows for better management of available resources during DN reconfiguration.

5.3. Simulations on IEEE 69-bus system

The initial configuration for the modified IEEE 69 bus system is shown in Fig. 20. The green star represents the slack node (PS), the black dotted lines are the open branches, while the continuous lines are the closed ones (the three different colors refer to the three feeders of the network). Fig. 21 shows in detail the multi-busbar structure of the PS: on the MV side, two busbars are present (nodes 2 and 3) that are connected by a breaker, which allows, if necessary, the two transformers to work in parallel. Then, the substation nodes (36, 4, 28) are connected to the above-mentioned busbars through two parallel bus-ties; lastly, lines 36–27, 4–5, and 28–29 are the $\mathbb{B}^0$ branches. The 38 branches connected to nodes with more than three edges linked have been considered maneuverable. The initial load, generation, and net real power profiles are plotted in Fig. 22.

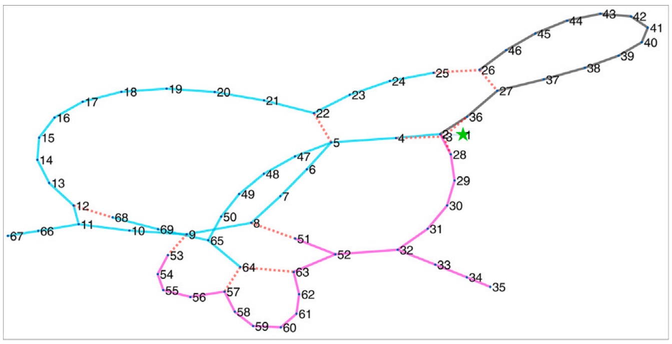

Fig. 20. IEEE 69-bus system: initial configuration.

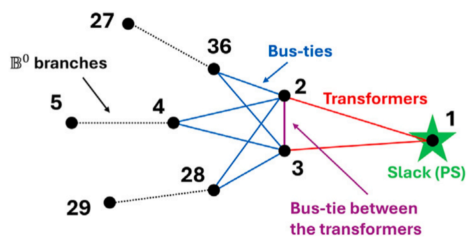

Fig. 21. Detail of the PS nodes area.

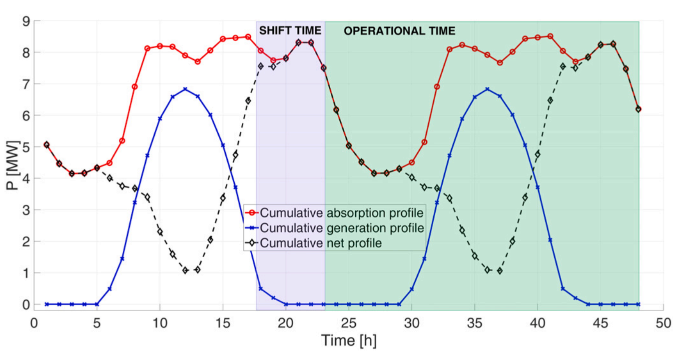

Fig. 22. Modified IEEE 69-bus system: load, generation, and net real power profiles.

Since the details of the proposed functionalities were shown using the IEEE 12-bus system, this larger-sized DN is used to test the global properties of the proposed approach: both $OF_{\#1}$ and $OF_{\#2}$ are evaluated by progressively increasing the maximum number of feasible switches allowed during the SHIFT TIME. As in the previous case, it has been assumed that the reconfiguration can begin two hours earlier; hence, only the number of maneuvers per hour has been modified. The maximum number of feasible switches (a $C - O$ maneuver pair) is thus iteratively increased by 1 until the objective function values stop improving from one iteration to the next.

Figs. 23 and 24 highlight the results for $OF_{\#1}$ and $OF_{\#2}$ optimization, respectively, together with the simulation time necessary to reach convergence. In both figures, the ideal value of the objective functions, obtained by neglecting the SHIFT TIME constraints is also represented. First, for both cases the simulation time increases as the maximum number of maneuvers increases, while remaining within an acceptable range. Then, the value of the two objective functions decreases as the maximum number of maneuvers increases, as the algorithm has more margin to define a better condition. In both cases, the objective functions don't reach the corresponding ideal values, due to the technical network constraints during SHIFT TIME; however, they get very close to the ideal values for

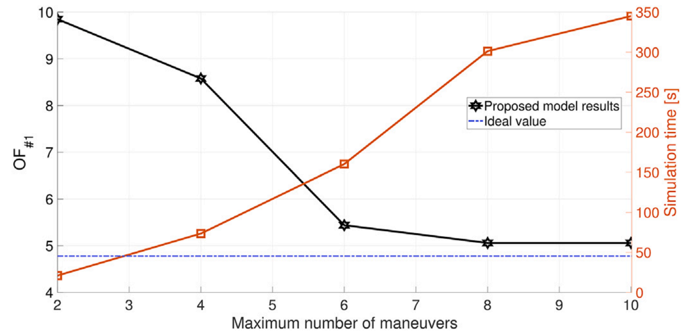

Fig. 23. IEEE 69-bus system: scalability of the proposed algorithm for $OF_{\#1}$.

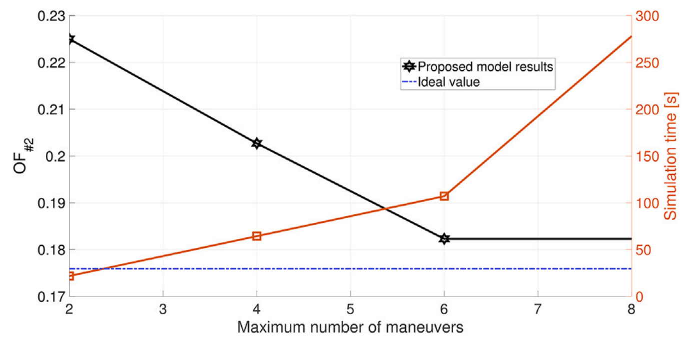

Fig. 24. IEEE 69-bus system: scalability of the proposed algorithm for $OF_{\#2}$.

a realistic value of the maximum number of maneuvers, with a difference of 5.54 % for $OF_{\#1}$ with 6 maneuvers and 3.51 % for $OF_{\#2}$ with 8 maneuvers.

These results highlight the scalability and computational efficiency of the proposed method. Despite the increased dimensionality of the 69-bus test system and the introduction of realistic operational constraints (including the modeling of configuration shift steps and RVC limits) the model is able to converge in all scenarios tested. Simulation times remain within a few minutes even as the number of allowed maneuvers increases, confirming the tractability of the MILP formulation for practical DN sizes. Moreover, the sequential improvement in the objective functions with a limited number of feasible switches demonstrates the algorithm's ability to efficiently exploit additional degrees of freedom without excessive computational burden, confirming the ability of the proposed method to be implemented in large-scale DNs for real-time implementation.

6. Conclusions

In this work, a novel methodology for the optimal reconfiguration of DN in presence of RES has been implemented, formulated as a MILP program. Starting from an initial configuration, the goal is to determine a new, optimal, one according to a defined objective function, assuming to know the future load and generation profiles over a multi-temporal period. After defining (i) how early before the period to optimize the shift between the configurations must start and (ii) how many maneuvers are possible to perform per each time step, the algorithm also defines the optimal sequence of maneuvers during the shift, while guaranteeing connectivity, radiality, and compliance with the network constraints, such as voltage and current limits and the Rapid Voltage Change (RVC). In this way, practical challenges, such as equipment stress and security risks during the transition period, are taken into account. Moreover, an efficient formulation to include bus-ties and breakers as zero-impedance branches is proposed, which allows a more practical representation of the physical structure of the DN and greater flexibility. Lastly, improved versions of two promising objective functions found in the literature (feeder balancing and security of supply maximization) have been formulated. The proposed algorithm has been tested on the IEEE 12-bus and IEEE 69-bus systems in order to verify the impact of the proposed innovative features. In particular, results highlight the importance of considering RVC constraints, showing that neglecting modeling of the shift between the configurations can lead to theoretically optimal configurations that, in practice, are infeasible. Furthermore, the inclusion of bus-tie modeling enhances feeder load distribution and optimizes the use of existing infrastructure. Future studies should extend this methodology to address stochastic variations in renewable energy generation and demand profiles to improve its robustness under uncertainty. This implementation will be able to be handled by various strategies, such as stochastic and robust optimization; although this development will lead to different numerical results than those obtained when considering deterministic generation and load profiles, it does not change the overall structure of the algorithm. Moreover, strategies to reduce the size of the problem, especially in the path-formulation, should be investigated, in order to achieve lower computational time for the analysis of larger DNs. Lastly, the present model assumes that only one switching operation can be performed at each time step. Future work may include the incorporation of operator availability constraints or parallel maneuver execution, linking the temporal modeling of maneuvers to the number of available working teams or remote-controlled breakers.

CRediT authorship contribution statement

Riccardo Nebuloni: Software, Writing – original draft, Formal analysis, Investigation, Conceptualization, Methodology. **Valentin Ilea:** Visualization, Methodology, Writing – review & editing, Supervision, Investigation, Conceptualization, Formal analysis. **Cristian Bovo:** Project administration, Conceptualization, Supervision, Visualization, Resources, Formal analysis, Writing – review & editing. **Alberto Berizzi:** Writing – review & editing, Supervision. **Carlo Arrigoni:** Software, Validation, Project administration, Supervision, Resources. **Filippo Re:** Supervision, Validation, Resources, Project administration. **Roberto Bonera:** Resources, Validation, Software.

Declaration of competing interest

The authors declare that they have no known competing financial interests or personal relationships that could have appeared to influence the work reported in this paper.

Appendix A. Comments on the monitoring of the possible violations

To improve algorithm efficiency, voltage and current bounds are not monitored across all network components. Instead, the following are initially monitored:

- Branches where $\frac{I_{j,t}}{I_j^{\mathrm{MAX}}} \geq \tilde{\tau}$, with $\tilde{\tau}$ set to 0.8 in this study.
- For each feeder, nodes with the minimum and maximum voltage magnitudes.

After each optimization, violations are re-evaluated:

- If no violations are found, the algorithm terminates.
- If new violations occur, the affected nodes and branches are added to the monitored set.
- Optimization continues iteratively until all violations are resolved.

Data availability

Data will be made available on request.

References

[1] M. Hannan, A. Al-Shetwi, R. Begum, S. Young, M. Hoque, P. Ker, M. Mansur, K. Alzaareer, The value of thermal management control strategies for battery energy storage in grid decarbonization: issues and recommendations, J. Clean. Prod. 276 (2020).

[2] EU Parliament and Council, Renewable Energy Directive 2018, 2018.

[3] EU Parliament and Council, Directive of on the Promotion of Clean and Energy-Efficient Road Transport Vehicles, 2019.

[4] E. Daccò, D. Falabretti, V. Ilea, M. Merlo, R. Nebuloni, M. Spiller, Decentralised voltage regulation through optimal reactive power flow in distribution networks with dispersed generation, Electricity 5 (1) (2024).

[5] V. Ilea, R. Nebuloni, C. Arrigoni, F. Re, C. Bovo, R. Bonera, A sensitivity-based linear model for optimal dispatch of local flexibility, in: 2024 20th International Conference on the European Energy Market (EEM), 2024, pp. 1–6.

[6] D. Andreotti, M. Spiller, A. Scrocca, F. Bovera, G. Rancilio, Modeling and analysis of bess operations in electricity markets: prediction and strategies for day-ahead and continuous intra-day markets, Sustainability 16 (18) (2024).

[7] G. Taromboli, T. Soares, J. Villar, M. Zatti, F. Bovera, Impact of different regulatory approaches in renewable energy communities: a quantitative comparison of European implementations, Energy Policy 195 (2024) 114399.

[8] A. Di Martino, S.M. Miraftabzadeh, M. Longo, Strategies for the modelisation of electric vehicle energy consumption: a review, Energies 15 (21) (2022).

[9] C.M. Caminiti, L.G. Brigatti, M. Spiller, G. Rancilio, M. Merlo, Unlocking grid flexibility: leveraging mobility patterns for electric vehicle integration in ancillary services, World Electr. Veh. J. 15 (9) (2024).

[10] S. Borgosano, D. Martini, M. Longo, F. Foiadelli, Electrifying urban transportation: a comparative study of battery swap stations and charging infrastructure for taxis in Chicago, IEEE Access 12 (2024) 48017–48026.

[11] R. Nebuloni, L. Meraldi, L. Moretti, V. Ilea, C. Bovo, A. Berizzi, P. Raboni, A real-time cycle counting method for battery degradation calculation in milp models, in: 2023 EEEIC, 2023.

[12] R. Nebuloni, L. Meraldi, C. Bovo, V. Ilea, A. Berizzi, S. Sinha, R.B. Tamirisakandala, P. Raboni, A hierarchical two-level milp optimization model for the management of grid-connected bess considering accurate physical model, Appl. Energy 334 (2023).

[13] X. Wang, Q. Kang, X. Wei, L. Guo, Z. Liang, Resilience assessment and recovery of distribution network considering the influence of communication network, Int. J. Electr. Power Energy Syst. 152 (2023) 109280.

[14] R. Nebuloni, V. Ilea, A. Berizzi, C. Bovo, C. Arrigoni, F. Corti, B. Conte, R. Bonera, Optimal management of flexibility services in lv distribution grids, in: 27th International Conference on Electricity Distribution (CIRED 2023), 2023.

[15] C.A. Cortes, S.F. Contreras, M. Shahidehpour, Microgrid topology planning for enhancing the reliability of active distribution networks, IEEE Trans. Smart Grid 9 (6) (2018).

[16] O. Badran, S. Mekhilef, H. Mokhlis, W. Dahalan, Optimal reconfiguration of distribution system connected with distributed generations: a review of different methodologies, Renew. Sustain. Energy Rev. 73 (2017) 854–867.

[17] A. Bosisio, M. Moncecchi, A. Morotti, M. Merlo, Machine learning and gis approach for electrical load assessment to increase distribution networks resilience, Energies 14 (14) (2021).

[18] C. Bovo, V. Ilea, M. Subasic, F. Zanellini, C. Arrigoni, R. Bonera, Improvement of observability in poorly measured distribution networks, in: 2014 Power Systems Computation Conference, 2014.

[19] B. Sultana, M. Mustafa, U. Sultana, A.R. Bhatti, Review on reliability improvement and power loss reduction in distribution system via network reconfiguration, Renew. Sustain. Energy Rev. 66 (2016) 297–310.

[20] M.R. Behbahani, A. Jalilian, A. Bahmanyar, D. Ernst, Comprehensive review on static and dynamic distribution network reconfiguration methodologies, IEEE Access 12 (2024) 9510–9525.

[21] A. Mishra, M. Tripathy, P. Ray, A survey on different techniques for distribution network reconfiguration, J. Eng. Res. (Ponta. Grossa) 12 (1) (2024) 173–181.

[22] R. Taleski, D. Rajicic, Distribution network reconfiguration for energy loss reduction, IEEE Trans. Power Syst. 12 (1) (1997) 398–406.

[23] J.S. Savier, D. Das, Impact of network reconfiguration on loss allocation of radial distribution systems, IEEE Trans. Power Deliv. 22 (4) (2007) 2473–2480.

[24] T.T. Nguyen, A novel metaheuristic method based on artificial ecosystem-based optimization for optimization of network reconfiguration to reduce power loss, Soft Comput. (2021).

[25] A.M. Helmi, R. Carli, M. Dotoli, H.S. Ramadan, Efficient and sustainable reconfiguration of distribution networks via metaheuristic optimization, IEEE Trans. Autom. Sci. Eng. 19 (1) (2022) 82–98.

[26] M.T.G. Jahani, P. Nazarian, A. Safari, M. Haghifam, Multi-objective optimization model for optimal reconfiguration of distribution networks with demand response services, Sustain. Cities Soc. 47 (2019) 101514.

[27] F.J. Ruiz-Rodríguez, S. Kamel, M.H. Hassan, J.A. Dueñas, Optimal reconfiguration of distribution systems considering reliability: introducing long-term memory component aeo algorithm, Expert Syst. Appl. 249 (2024) 123467.

[28] P.C. Ramaswamy, J. Tant, J.R. Pillai, G. Deconinck, Novel methodology for optimal reconfiguration of distribution networks with distributed energy resources, Electr. Power Syst. Res. 127 (2015) 165–176.

[29] Y.-Y. Fu, H.-D. Chiang, Toward optimal multiperiod network reconfiguration for increasing the hosting capacity of distribution networks, IEEE Trans. Power Deliv. 33 (5) (2018).

[30] A. Borghetti, A mixed-integer linear programming approach for the computation of the minimum-losses radial configuration of electrical distribution networks, IEEE Trans. Power Syst. 27 (3) (2012).

[31] R.S. Ferreira, C.L.T. Borges, M.V.F. Pereira, A flexible mixed-integer linear programming approach to the ac optimal power flow in distribution systems, IEEE Trans. Power Syst. 29 (5) (2014).

[32] F. Llorens-Iborra, J. Riquelme-Santos, E. Romero-Ramos, Mixed-integer linear programming model for solving reconfiguration problems in large-scale distribution systems, Electr. Power Syst. Res. 88 (2012).
[33] M. Baran, F. Wu, Network reconfiguration in distribution systems for loss reduction and load balancing, IEEE Trans. Power Deliv. 4 (2) (1989) 1401–1407.
[34] M. Kashem, G. Jasmon, V. Ganapathy, A new approach of distribution system reconfiguration for loss minimization, Int. J. Electr. Power Energy Syst. 22 (4) (2000) 269–276.
[35] H.-D. Chiang, R. Jean-Jumeau, Optimal network reconfigurations in distribution systems. i. A new formulation and a solution methodology, IEEE Trans. Power Deliv. 5 (4) (1990) 1902–1909.
[36] I. Roytelman, V. Melnik, S. Lee, R. Lugtu, Multi-objective feeder reconfiguration by distribution management system, IEEE Trans. Power Syst. 11 (2) (1996) 661–667.
[37] Ž.N. Popović, N.V. Kovački, Multi-period reconfiguration planning considering distribution network automation, Int. J. Electr. Power Energy Syst. 139 (2022).
[38] Z. Tian, W. Wu, B. Zhang, A. Bose, Mixed-integer second-order cone programing model for var optimisation and network reconfiguration in active distribution networks, IET Gener. Transm. Distrib. 10 (8) (2016) 1938–1946.
[39] E. Ramos, A. Exposito, J. Santos, F. Iborra, Path-based distribution network modeling: application to reconfiguration for loss reduction, IEEE Trans. Power Syst. 20 (2) (2005).
[40] S. Bahrami, Y.C. Chen, V.W.S. Wong, Dynamic distribution network reconfiguration with generation and load uncertainty, IEEE Trans. Smart Grid 15 (6) (2024) 5472–5484.
[41] H.-D. Chiang, M. Baran, On the existence and uniqueness of load flow solution for radial distribution power networks, IEEE Trans. Circuits Syst. 37 (3) (1990) 410–416.
[42] R. Sarfi, M. Salama, A. Chikhani, A survey of the state of the art in distribution system reconfiguration for system loss reduction, Electr. Power Syst. Res. 31 (1) (1994) 61–70.
[43] J. Zhang, C. Liu, X. Li, H.-L. Zhen, M. Yuan, Y. Li, J. Yan, A survey for solving mixed integer programming via machine learning, Neurocomputing 519 (2023) 205–217.
[44] R.S. Rao, K. Ravindra, K. Satish, S.V.L. Narasimham, Power loss minimization in distribution system using network reconfiguration in the presence of distributed generation, IEEE Trans. Power Syst. 28 (1) (2013) 317–325.
[45] S. Kalambe, G. Agnihotri, Loss minimization techniques used in distribution network: bibliographical survey, Renew. Sustain. Energy Rev. 29 (2014) 184–200.
[46] P. Ushashree, K.S. Kumar, Power system reconfiguration in distribution system for loss minimization using optimization techniques: a review, Wirel. Pers. Commun. 128 (3) (2023) 1907–1940.
[47] P.C. Sekhar, R.A. Deshpande, V. Sankar, Evaluation and improvement of reliability indices of electrical power distribution system, in: 2016 National Power Systems Conference (NPSC), 2016, pp. 1–6.
[48] D. Tylavsky, P. Crouch, L. Jarriel, J. Singh, R. Adapa, The effects of precision and small impedance branches on power flow robustness, IEEE Trans. Power Syst. 9 (1) (1994) 6–14.
[49] F. Milano, On the modelling of zero impedance branches for power flow analysis, IEEE Trans. Power Syst. 31 (4) (2016).
[50] A. Monticelli, A. Garcia, Modeling zero impedance branches in power system state estimation, IEEE Trans. Power Syst. 6 (4) (1991) 1561–1570.
[51] N.A. Belda, R.P.P. Smeets, R.M. Nijman, Experimental investigation of electrical stresses on the main components of hvdc circuit breakers, IEEE Trans. Power Deliv. 35 (6) (2020) 2762–2771.
[52] International Electrotechnical Commission, IEC 61000-3-3: Limitation of Voltage Changes, Voltage Fluctuations and Flicker in Public Low-Voltage Supply Systems, 2013.
[53] F. Capitanescu, L.F. Ochoa, H. Margossian, N.D. Hatziargyriou, Assessing the potential of network reconfiguration to improve distributed generation hosting capacity in active distribution systems, IEEE Trans. Power Syst. 30 (1) (2015) 346–356.
[54] A. Borghetti, C.A. Nucci, M. Paolone, G. Ciappi, A. Solari, Synchronized phasors monitoring during the islanding maneuver of an active distribution network, IEEE Trans. Smart Grid 2 (1) (2011) 82–91.
[55] R. Baldick, The generalized unit commitment problem, IEEE Trans. Power Syst. 10 (1) (1995) 465–475.
[56] T. Krishnaiyan, A. Subramanian, B. Andreas, N. Takao, Handbook of Graph Theory, Combinatorial Optimization, and Algorithms., Chapman & Hall, 2016.
[57] L. Chua, C. Desoer, E. Kuh, Linear and Nonlinear Circuits, McGraw-Hill Book Company, 1987.
[58] S.M. Ismael, S.H.A. Aleem, A.Y. Abdelaziz, A.F. Zobaa, State-of-the-art of hosting capacity in modern power systems with distributed generation, Renew. Energy 130 (2019) 1002–1020.
[59] R.N. Sengupta, A. Gupta, J. Dutta, Decision Sciences: Theory and Practice, CRC Press, 2016.
[60] V. da Costa, N. Martins, J. Pereira, Developments in the newton raphson power flow formulation based on current injections, IEEE Trans. Power Syst. 14 (4) (1999) 1320–1326.
[61] P. Garcia, J. Pereira, S. Carneiro, V. da Costa, N. Martins, Three-phase power flow calculations using the current injection method, IEEE Trans. Power Syst. 15 (2) (2000) 508–514.
[62] J. Bisschop, Optimization Modelling, 2020.
[63] J.S. Giraldo, P.P. Vergara, J.C. López, P.H. Nguyen, N.G. Paterakis, A linear ac-opf formulation for unbalanced distribution networks, IEEE Trans. Ind. Appl. 57 (5) (2021).
[64] M. Barni, F. Buti, F. Bartolini, V. Cappellini, A quasi-euclidean norm to speed up vector median filtering, IEEE Trans. Image Process. 9 (10) (2000).
[65] A. Garces, A linear three-phase load flow for power distribution systems, IEEE Trans. Power Syst. 31 (1) (2016).
[66] R. Marconato, Electric Power Systems, vol. 2, CEI, 2008.
[67] A. Eltamaly, et al., “Reliability/Security of distribution system network under supporting by distributed generation, Energy Sci., 04 2019).
[68] A.F.A. Kadir, A. Mohamed, H. Shareef, M. Wanik, Optimal placement and sizing of distributed generations in distribution systems for minimizing losses and thd v using evolutionary programming, Turk. J. Electr. Eng. Comput. Sci. 21 (2013).
[69] V. Ilea, C. Bovo, D. Falabretti, M. Merlo, C. Arrigoni, R. Bonera, M. Rodolfi, Voltage control methodologies in active distribution networks, Energies 13 (12) (2020).
[70] European Union Science Lab, PVGIS online tool, 2024 [Online]. Available: https://joint-research-centre.ec.europa.eu/photovoltaic-geographical-information-system-pvgis_en.
[71] Italian Electrotechnical Committee (CEI), CEI 0-16: Technical Rule for the Connection of Active and Passive Users to the MV and HV Electricity Distribution Networks, 2022.